

Supporting Information

A large axial magnetic anisotropy in trigonal bipyramidal Fe(II)

Moya A. Hay,^a Arup Sarkar^b, Gavin A. Craig,^{‡a} Katie. E. R. Marriott,^a Claire Wilson,^a Gopalan Rajaraman^{b*} and Mark Murrie^{a,*}

^aSchool of Chemistry, University of Glasgow, Glasgow, G12 8QQ (UK)

^bDepartment of Chemistry, Institute of Technology Bombay, Powai, Mumbai, Maharashtra, 400 076
(India) Email: rajaraman@chem.iitb.ac.in

[‡] Present address: Department of Pure and Applied Chemistry, University of Strathclyde, Glasgow,
UK.

mark.murrie@glasgow.ac.uk

Contents

Physical Methods and Experimental Details	1
Table S1 Crystal Data and Structure Refinement Parameters	2
Table S2 <i>SHAPE</i> studies	2
Figure S1 Powder X-ray Diffraction of 1	3
Additional Information Corresponding to the Fit of Magnetic Data.....	3
Figure S2 Independent fits of $\chi_M T$ vs. T and M vs. H	4
Figure S3 Survey of D with g_{xy} and g_z	4
Figure S4 Frequency-dependence of the in-phase component of the ac susceptibility at 2 K in Hdc = 0 – 5000 Oe.....	5
Figure S5 Argand Diagram and normalised maximum χ'' values for the HF and LF relaxation paths. 5	
Figure S6 Variable temperature frequency-dependence of the in-phase component of the ac susceptibility at Hdc = 600 Oe.....	6
Figure S7 Variable temperature frequency-dependence of the ac susceptibility at Hdc = 2500 and 5000 Oe.....	6
Figure S8 Argand diagram for temperature dependent ac studies.	7
Figure S9 Arrhenius plots with fits via straight line approximations.	8
Figure S10 Field dependence of the inverse of the relaxation rates.....	8
Figure S11 Fit of relaxation rates at Hdc = 600 and 2500 Oe.....	9
Table S3 ZFS parameters of previously reported Fe(II) complexes that exhibited slow relaxation of magnetisation	10
Computational Details.....	10
Figure S12 NEVPT2 energy spectrum.....	11
Table S4 NEVPT2 computed electronic states	11
Table S5 Diagonalised eigenvalues of the first five spin-orbit states.....	12
References.....	12

Physical Methods

Air-sensitive elemental analysis (EA) was performed on **1** via the Elemental Analysis Service, University of Strathclyde. IR spectra were collected using a Shimadzu FTIR spectrometer in the range 4000-600 cm⁻¹. Crystallographic data was collected for **1** at 100 K using Mo-K α radiation ($\lambda = 0.71073 \text{ \AA}$). For **1** a Bruker APEXII CCD diffractometer with an Oxford Cryosystems n-Helix low-temperature device mounted on a sealed tube generator was used. The structure was then solved using *Superflip*¹ and refined using full-matrix least-squares refinement using *Olex*² software.^{2,3} The powder X-ray pattern was collected on a PANalytical XPert MPD, with Cu K $\alpha 1$ radiation at ambient temperature over a range of $5^\circ < 2\theta < 50^\circ$ using a step size of 0.0167° . The calculated pattern was generated from *Mercury*⁴ using the .cif of the crystal structure at 100 K. All magnetic measurements were carried out on powdered crystalline samples restrained in eicosane to prevent torqueing or reorientation using a Quantum Design MPMS-XL SQUID magnetometer. Data were corrected for the diamagnetic contribution of the sample holder and eicosane by measurements, and for the diamagnetism of the compound ($\chi_{DIA} = 2.58 \cdot 10^{-4} \text{ cm}^3 \cdot \text{mol}^{-1}$).

Experimental Details

[Fe(MDABCO)₂Cl₃]·[ClO₄] (**1**): A solution of [MDABCO][I] (0.26 g, 1 mmol) and NaClO₄ (0.12 g, 1 mmol) was added to a solution of FeCl₂ (0.13 g, 1 mmol) in methanol (50 ml) to form a pale yellow solution. The yellow solution was then stirred for three hours at room temperature after which a deeper yellow solution was obtained. Vapour diffusion with diethyl ether gave colourless single crystals of **1** suitable for X-ray diffraction after three days. Yield of product 25 % (96 mg). IR (ν in cm⁻¹): 3426 (w), 3385 (w), 2974 (w), 1593 (w), 1470 (m), 1352 (w), 1325 (w), 1200 (w), 1076 (s), 1053 (s), 1016 (m), 990 (w), 918 (m), 841 (m), 797 (m), 689 (w), 621 (s). EA analysis: (C₁₄H₃₀Cl₄FeN₄O₄·0.5H₂O) [%], found: C 31.88, H 5.56, N 11.01; calc: C 32.02, H 5.95, N 10.67.

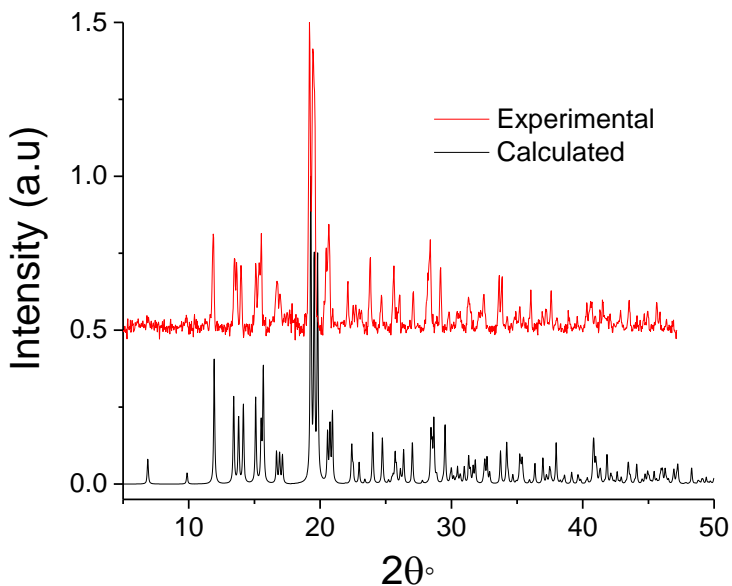
Table S1 Crystal Data and Structure Refinement Parameters

1	
Empirical formula	C ₁₄ H ₃₀ Cl ₄ FeN ₄ O ₄
Formula weight	516.07
Temperature / K	100(2)
Crystal system	orthorhombic
Space group	Pca2 ₁
<i>a</i> / Å	12.504(3)
<i>b</i> / Å	12.830(3)
<i>c</i> / Å	13.185(3)
α / °	90
β / °	90
γ / °	90
Volume / Å ³	2115.3(8)
<i>Z</i>	4
ρ_{calc} g / cm ³	1.621
μ / mm ⁻¹	1.246
<i>F</i> (000)	1072.0
Crystal size / mm ³	0.1 × 0.1 × 0.05
Radiation	MoKα ($\lambda = 0.71073$)
2θ range for data collection / °	3.174 to 51.436
Index ranges	-15 ≤ <i>h</i> ≤ 15, -13 ≤ <i>k</i> ≤ 15, -16 ≤ <i>l</i> ≤ 16
Reflections collected	20994
Independent reflections	4010 [$R_{\text{int}} = 0.1208$, $R_{\text{sigma}} = 0.1021$]
Data/restraints/parameters	4010/1/247
Goodness-of-fit on <i>F</i> ²	1.028
Final R indexes [<i>I</i> ≥ 2σ (<i>I</i>)]	$R_1 = 0.0448$, $wR_2 = 0.0840$
Final R indexes [all data]	$R_1 = 0.0895$, $wR_2 = 0.0996$
Largest diff. peak/hole / e Å ⁻³	0.50/-0.53
Flack parameter	0.01(4)

Table S2 Results from *SHAPE* studies for **1** with the lowest CShM value highlighted in purple signifying the closest geometry of the complex.^{5,6}

Shape	Symmetry	CShM Values
Pentagon	D _{5h}	35.998
Vacant Octahedron	C _{4v}	6.604
Trigonal Bipyramide	D_{3h}	0.057
Spherical Square Pyramid	C _{4v}	4.501
Johnson Trigonal Bipyramide	D _{3h}	3.130

Figure S1 Calculated (black) and the experimentally obtained (red) powder diffraction pattern for **1** confirming phase purity of the sample.



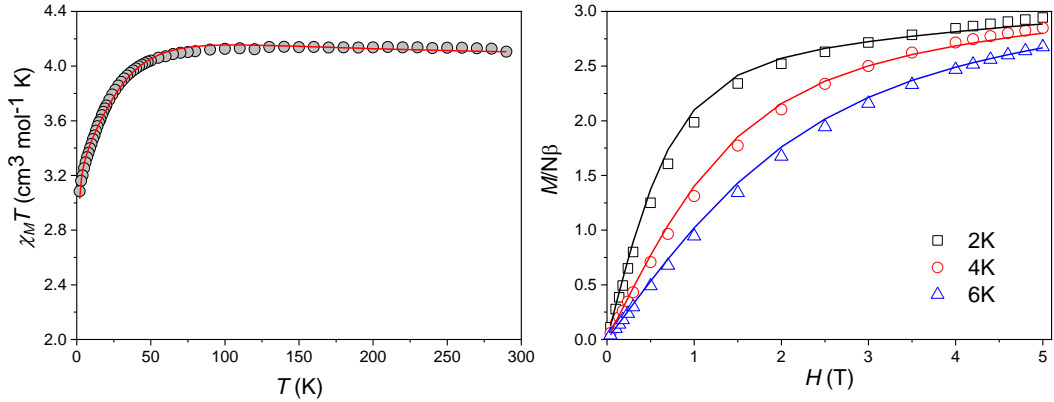
Additional Information Corresponding to the Fit of Magnetic Data

When fitting M vs. H and $\chi_M T$ vs. T simultaneously as described in the main text, the temperature independent paramagnetic (*TIP*) contribution to the susceptibility of $0.32 \times 10^{-3} \text{ cm}^3 \text{ mol}^{-1}$ was determined from the fit and required to replicate the high temperature susceptibility data. This value is reasonable, being slightly lower than that predicted for Fe(II) in an octahedral environment.⁷ The second parameter determined from the fit was a contribution to the susceptibility from intermolecular interactions (zJ) with a value of $-0.024 \text{ cm}^3 \text{ mol}^{-1}$ which was required in order to replicate the low temperature susceptibility data and was necessary for the fit to converge.

Difficulties in fitting the data simultaneously are evident from the deviation of the M vs. H data at high fields in Fig. 3 of the communication. In the following discussion each dataset was instead subject to a fit independently and the rhombic ZFS parameter E was approximated to 0, as expected for an axial system.

For the $\chi_M T$ vs. T data (see Figure S2, left), D was fixed (-27.5 cm^{-1}) as determined from the *ab initio* studies while g_{xy} ($= 2.17$), g_z ($= 2.58$) and zJ ($= -0.015 \text{ cm}^{-1}$) were obtained from the fit. For the M vs. H data (see Figure S2, right), we show the effect of using a fixed isotropic g -value (2.6) and fitting D ($= -27.7 \text{ cm}^{-1}$).

Figure S2 $\chi_M T$ vs. T data (left) and M vs. H data (right) where solid lines correspond to the fits of the data treated individually as explained above.



Next, a survey was conducted on the g -tensors (using g_{xy} and g_z taking the approximation that **1** is axial) and the axial ZFS parameter D taking into consideration both the M vs. H and $\chi_M T$ vs. T datasets simultaneously. The survey function in *PHI* sweeps the values within defined ranges providing a residual error for each parameter.⁸ The minima can be identified in Figure S3 by the areas darkest in colour where for $g_z \sim 2.75$, $D/3 \approx -13 \text{ cm}^{-1}$ and for $g_{xy} \sim 2.15$, $D/3 \approx -10 \text{ cm}^{-1}$ (*note the use of $D/3$ in the survey plots, rather than D*). This shows that both the M vs. H and $\chi_M T$ vs. T datasets are in good agreement with the large D parameter and the g_{xy} and g_z values.

Figure S3 Survey (in 500 steps) of $D/3$ between -5 and -15 cm^{-1} and the g_z parameter between $2.2 - 3.0$ (left) and the g_{xy} parameter between $1.9 - 2.5$ (right) with the residual value for the survey demonstrated by the contour map where blue represents the local minimum. The full M vs. H and $\chi_M T$ vs. T data sets were used simultaneously for the survey.

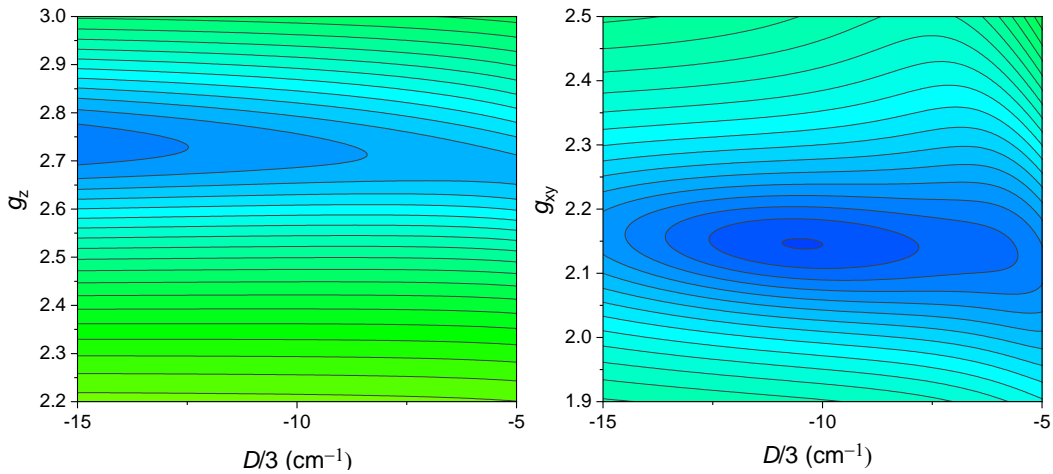


Figure S4 Frequency-dependence of the in-phase component (χ') of the alternating-current (ac) susceptibility in direct-current (dc) fields ranging between $H_{dc} = 0 - 5000$ Oe at 2 K.

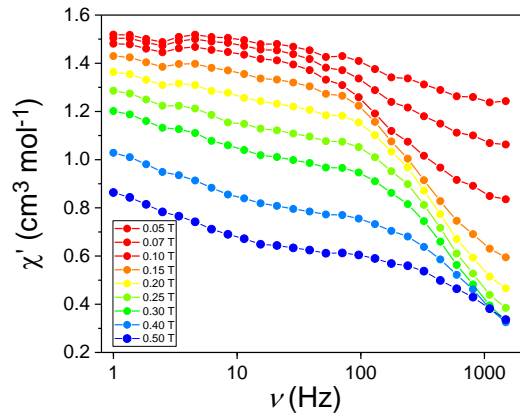


Figure S5 Argand Diagram (χ' vs. χ'') where the solid lines correspond to the fit of the data (left) and normalised maximum χ'' value against applied field (right) for the HF relaxation path shown in red and the LF in blue.

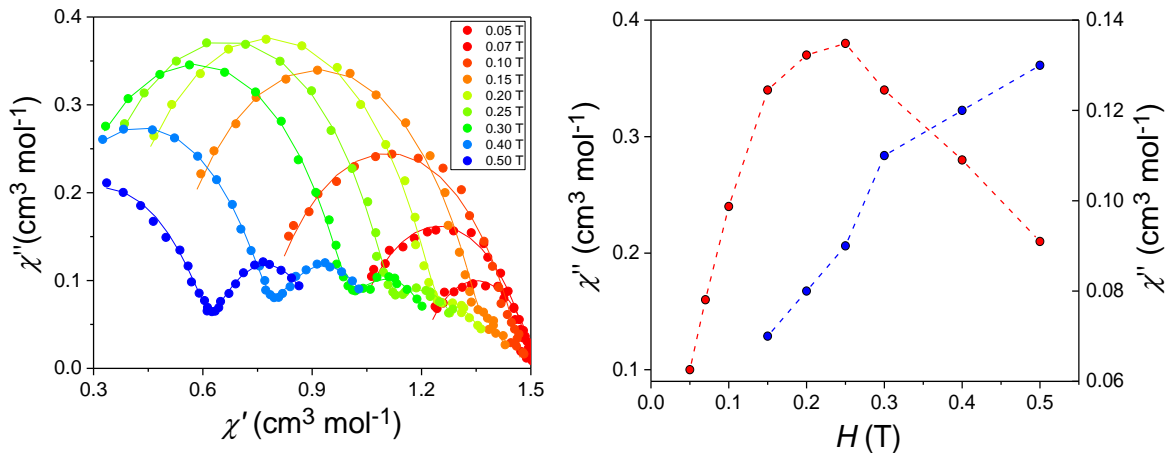


Figure S6 Frequency-dependence of the in-phase component of the ac susceptibility at 600 Oe between 1.9 and 9 K. The solid lines correspond to the fit.

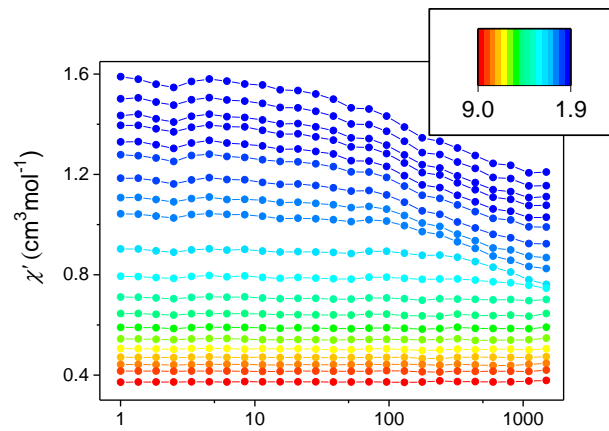


Figure S7 Frequency-dependence of the AC susceptibility at 2500 Oe (left) and 5000 Oe (right) between 1.9 and 9 K. The solid lines correspond to the fit.

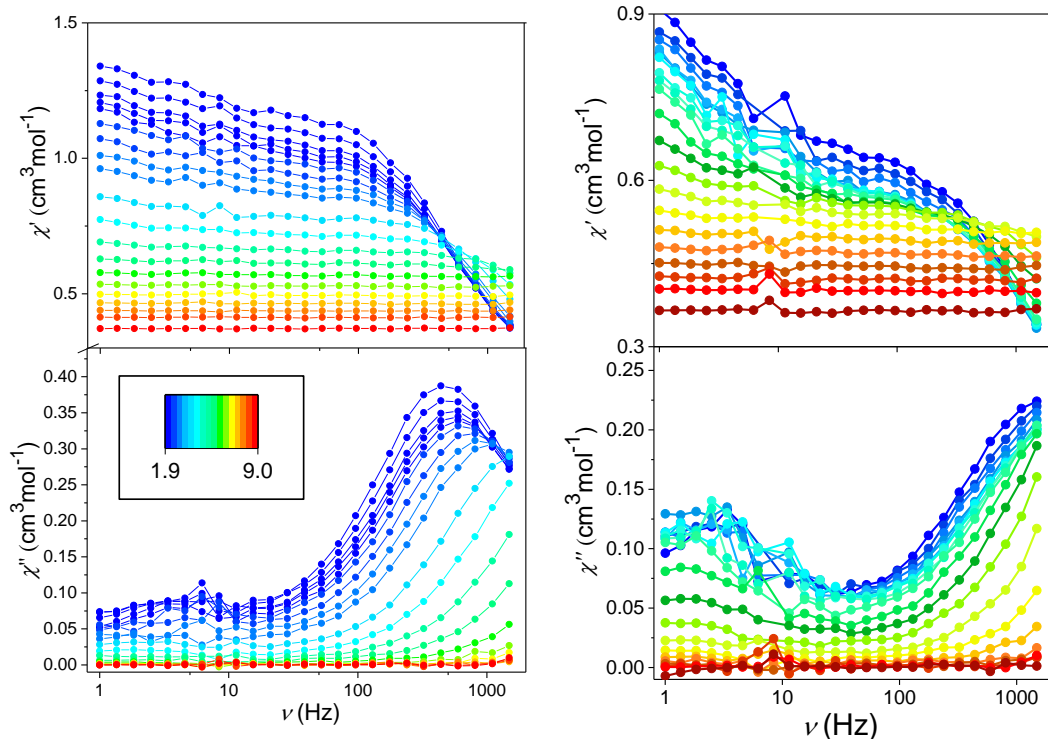
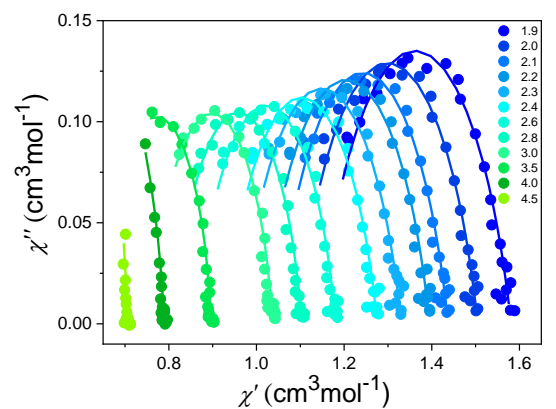
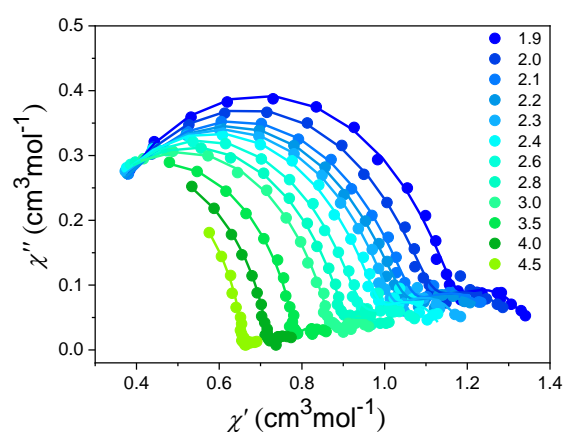


Figure S8 Argand diagram at 600 Oe (a), 2500 Oe (b), and 5000 Oe (c). Solid lines correspond to the fit (see main text for details).

a)



b)



c)

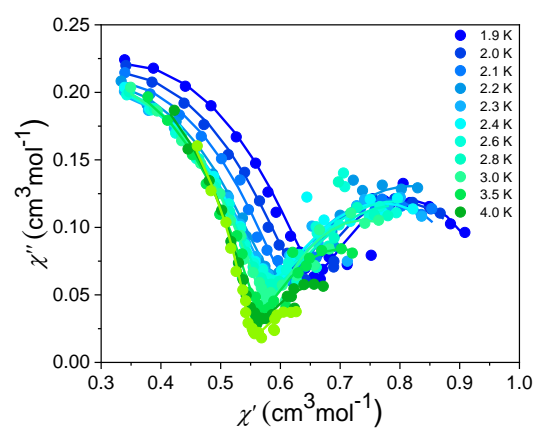


Figure S9 The Arrhenius plots ($\ln \tau$ vs. $1/T$) of the temperature-dependence of the relaxation rates at 600 Oe and 2500 Oe. Solid lines correspond to the crude fit of the data, see main text for discussion.

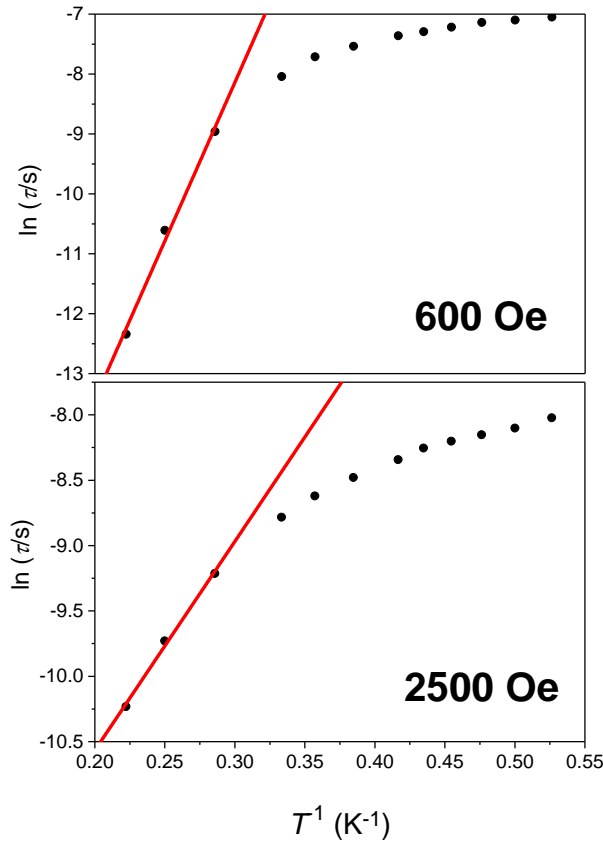


Figure S10 Field dependence of the inverse of the relaxation rates (τ^{-1}) for fields between 0.05 – 0.5 kOe Oe at 2 K where the solid red line corresponds to the fit including both a direct process and QTM giving $A = 182.35 (\pm 0.05) \times 10^2 s^{-1} kOe^{-2} K^{-1}$, $B_1 = 109.60 (\pm 0.04) \times 10 s^{-1}$ and $B_2 = 355.57 (\pm 2.56) \times 10^{-2} kOe^{-2}$.

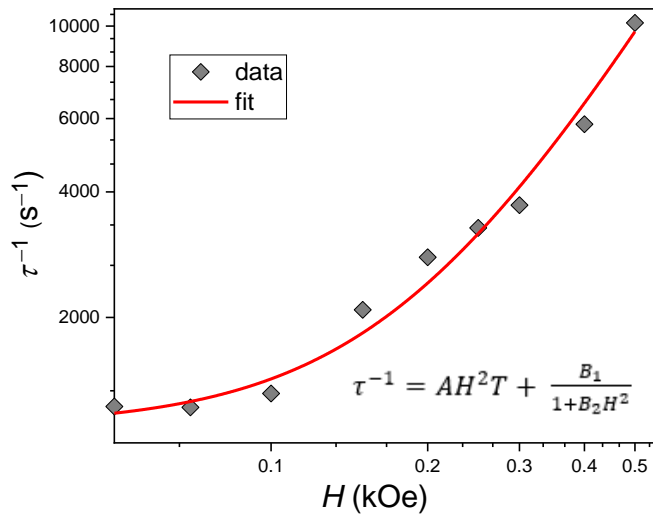


Figure S11 $1/\tau$ vs T plot with data collected at $H_{dc} = 600$ Oe and 2500 Oe with the fit given by the red and blue solid lines, respectively with parameters corresponding to the fits given in the main text. Note that the fit for $H_{dc} = 600$ Oe can be improved by including an Orbach term but it is not appropriate to include this term based on the estimated energy gap between ‘real’ states.

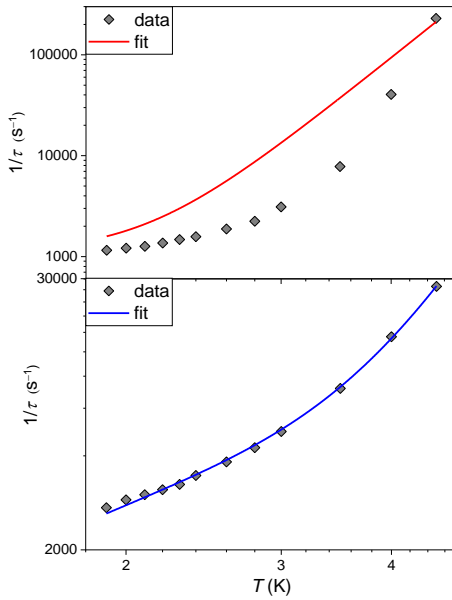


Table S3 A selection of previously reported Fe(II) complexes with D and E values presented where these had been deduced and method of determination denoted.

[Fe(C(SiMe ₃) ₃) ₂] ⁹	2 (C ₂)	Linear	-	-
Fe[N(SiMe ₃)(Dipp)] ₂ ⁹	2 (N ₂)	Linear	-	-
Fe[N(H)Ar'] ₂ ⁹	2 (N ₂)	Linear	-	-
Fe[OAr'] ₂ ⁹	2 (O ₂)	Linear	-	-
[⁵ CpFe(C ₆ H ₅ iPr ₃ -2,6)] ¹⁰	6 (C ₆)	Irregular	-51.36 ^[a]	0.32 ^[a]
[Fe(N(SiMe ₃) ₂) ₂ (PCy ₃)] ^{11,12}	3 (N ₃)	Trigonal Planar	-33 ^[a]	3.4 ^[a]
[Na(tpa ^{t-Bu})Fe] ¹³	4 (N ₄)	Trigonal Pyramidal	-48.0 ^[a]	0.4 ^[a]
[K(tpa ^{Mes})Fe] ^{13,14}	4 (N ₄)	Trigonal Pyramidal	-39.6 ^[a]	0.4 ^[a]
[Na(tpa ^{Ph})Fe] ¹³	4 (N ₄)	Trigonal Pyramidal	-26.2 ^[a]	5.0 ^[a]
PhB(MesIm) ₃ Fe-N=PPh ₃ ¹⁵	4 (C ₃ N)	Tetrahedral	-	-
[Fe(N ₂ _{mes}) ₂] ¹⁶	4 (N ₄)	Seesaw	-12.3 ^[a]	±0.01 ^[a]
[Fe(N ₂ Dipp) ₂] ¹⁶	4 (N ₄)	Tetrahedral	-16.9 ^[a]	±0.05 ^[a]
(NMe ₄)[Fe(MST)] ¹⁷	4 (N ₄)	Trigonal Pyramidal	-31.0 ^[a]	4.7 ^[a]
[Fe(N ₃ N)]·(Li(THF)) ¹⁸	4 (N ₄)	Trigonal Pyramidal	-7 ^[a]	±2 ^[a]
(NMe ₄)[Fe(MST)(OH ₂)] ¹⁷	5 (N ₄ O)	Trigonal Bipyramidal	8.7 ^[a]	2.4 ^[a]
[Fe(1-ptz) ₆]·(BF ₄) ₂ ¹⁹	6 (N ₆)	Octahedral	-14.8 ^[b]	-0.95 ^[b]
[Fe(mtz) ₆]·(CF ₃ SO ₃) ₂ ²⁰	6 (N ₆)	Octahedral	-24.9 ^[a]	-0.00011 ^[a]
[Fe(H ₂ L ^{N3O2Ph})Cl ₂]·0.5MeOH ²¹	7 (N ₃ O ₂ Cl ₂)	Pentagonal Dipyramid	-13.3 ^[a]	0.02 ^[a]
[Fe(H ₂ L ^{N3O2NH2})Cl ₂] ^{21,22}	7 (N ₃ O ₂ Cl ₂)	Pentagonal Bipyramid	-13.0 ^[a]	3.3 ^[a]
[Fe ^{II} L]·H ₂ O ²³	7 (N ₃ O ₄)	Pentagonal Bipyramid	-9.6 ^[a]	0.06 ^[a]
[Fe(dpphen) ₂]·(BF ₄) ₂ ²⁴	8 (N ₈)	Snub Disphenoid	-6.00 ^[a,b]	±0.04 ^[a,b]
Fe(L ₁) ₂]·(ClO ₄) ₂ ²⁵	8 (N ₄ O ₄)	Triangular dodecahedron	-11.7 ^[c]	0.08 ^[c]
Fe(L ₂) ₂]·(ClO ₄) ₂ ²⁶	8 (N ₄ O ₄)	Triangular dodecahedron	-11.7 ^[c]	0.06 ^[c]
Fe(L ₃) ₂]·(ClO ₄) ₂ ²⁶	8 (N ₄ O ₄)	Triangular dodecahedron	-3.1 ^[c]	0.06 ^[c]
Fe(L ₄) ₂]·(ClO ₄) ₂ ²⁶	8 (N ₄ O ₄)	Triangular dodecahedron	-2.7 ^[c]	0.5 ^[c]

Dipp = C₆H₃-2,6-Pr₂; Cp = cyclopentadienyl; tpa = tris(2-methylpyridyl)amine; N₃N = bis(N-trimethylsilyl-2-amidoethyl)amine; [H₃MST] = N,N',N"-{2,2',2"-nitrilotris-(ethane-2,1-diyl)}tris(2,4,6-trimethylbenzenesulfonamide); ptz = 1-propyltetrazole; mtz = 1-methyltetrazole; H₂L = 2,6-diacetylpyridine bis-benzoylhydrazone; dpphen = 2,9-bis(pyrazol-1-yl)-1,10-phenanthroline; L₁ and L₂ = 2,9-bis(carbomethoxy)-1,10-phenanthroline; L₃ and L₄ are 6,6'-dialkylcarboxylate-2,2'-bipyridine; H₂L = (3,12,18-triaza-6,9-dioxabicyclo[12.3.1]octadeca-1,14,16-triene -3,12-di-acetic acid). Crystal field parameters determined via [a] fit of the dc magnetic data; [b] High field EPR [c] *ab initio* calculations.

Computational Details

All the single point *ab initio* calculations have been performed using ORCA 4.0.0.2.²⁷ Configuration interactions have been computed by multi-determinant state-averaged CASSCF method. Scalar relativistic effect has been considered by including ZORA Hamiltonian during the calculations.²⁸ Also ZORA version of contracted basis set such as- ZORA-def2-TZVP for Fe, Cl; ZORA-def2-TZVP(-f) for N, O and ZORA-def2-SVP were used for rest of the atoms. An active space of six 3d electrons in five metal orbitals i.e., CAS(6,5) was chosen to optimize with 5 quintet and 45 triplet roots. Dynamic electron correlation was added on CASSCF wavefunction with NEVPT2

method. Spin-orbit coupling effect was included with quasi-degenerate perturbation theory (QDPT) approach and the final Spin-Hamiltonian parameters were computed using effective Hamiltonian approach (EHA).²⁹

Figure S12 NEVPT2 energy spectrum of 5 quintets and 45 triplets.

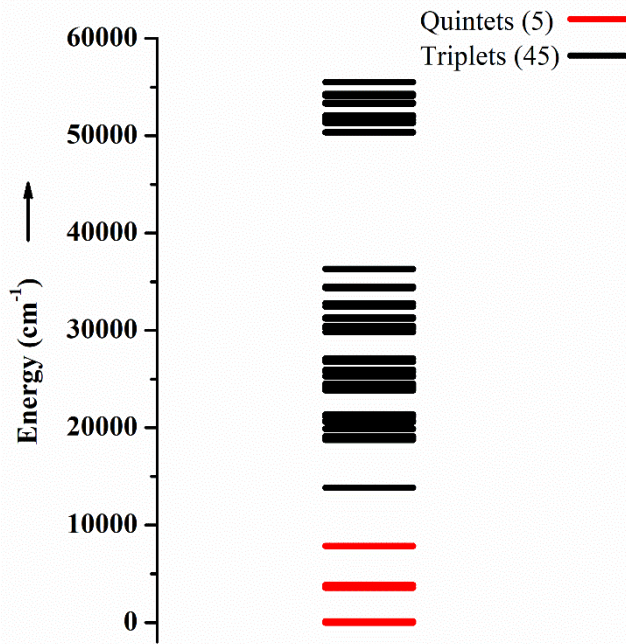


Table S4 NEVPT2 computed electronic states, the corresponding major electronic configurations and their individual contributions to the D and E values. Note that minor contributions are not shown and importantly, that the overall calculated D parameter comes from the diagonalisation of the whole D tensor rather than the summation of the contributions arising from individual states.

Energy states	NEVPT2 transition energy (cm^{-1})	Major CASSCF electronic configuration $d_{yz}d_{xz}d_{xy}d_{x^2-y^2}d_{z^2}$	Contribution to D (cm^{-1})	Contribution to E (cm^{-1})
${}^5E_x''$	0.0	2 1 1 1 1 (90%)	0.0	0.0
${}^5E_y''$	137.2	1 2 1 1 1 (89%)	-33.5	-0.00
${}^5E'$	3590.0	1 1 2 1 1 (54%)	1.6	-1.66
		1 1 1 2 1 (45%)		
${}^5A_1'$	3846.0	1 1 1 2 1 (55%)	1.3	1.29
		1 1 2 1 1 (45%)		
${}^5A_1'$	7844.1	1 1 1 1 2 (99%)	1.8	-1.8

Table S5 Diagonalised eigenvalues of the first five spin-orbit states.

Spin-Orbit states	Energy (cm ⁻¹)	Weightage	Spin multiplicity, root	M _S
1 st	0.00	66%	5,0	±2⟩
2 nd	0.08	66%	5,0	±2⟩
3 rd	70.44	80%	5,0	±1⟩
4 th	75.39	75%	5,0	±1⟩
5 th	119.85	98%	5,0	0⟩

References

- 1 L. Palatinus and G. Chapuis, *J. Appl. Crystallogr.*, 2007, **40**, 786–790.
- 2 O. V Dolomanov, L. J. Bourhis, R. J. Gildea, J. A. K. Howard and H. Puschmann, *J. Appl. Crystallogr.*, 2009, **42**, 339–341.
- 3 G. M. Sheldrick, *Acta Crystallogr. Sect. A*, 2015, **71**, 3–8.
- 4 C. F. Macrae, P. R. Edgington, P. McCabe, E. Pidcock, G. P. Shields, R. Taylor, M. Towler and J. Van De Streek, *J. Appl. Crystallogr.*, 2006, **39**, 453–457.
- 5 M. Pinsky and D. Avnir, *Inorg. Chem.*, 1998, **37**, 5575–5582.
- 6 D. Casanova, J. Cirera, M. Llunell, P. Alemany, D. Avnir and S. Alvarez, *J. Am. Chem. Soc.*, 2004, **126**, 1755–1763.
- 7 R. Boča, *A Handbook of Magnetochemical Formulae*, Elsevier, 2012.
- 8 A. S. and K. S. M. N. F. Chilton, R. P. Anderson, L. D. Turner, *J. Comput. Chem.*, 2013, **34**, 1164–1175.
- 9 J. M. Zadrozny, M. Atanasov, A. M. Bryan, C.-Y. Lin, B. D. Rekken, P. P. Power, F. Neese and J. R. Long, *Chem. Sci.*, 2013, **4**, 125–138.
- 10 D. Weismann, Y. Sun, Y. Lan, G. Wolmershäuser, A. K. Powell and H. Sitzmann, *Chem. – A Eur. J.*, 2011, **17**, 4700–4704.
- 11 P.-H. Lin, N. C. Smythe, S. I. Gorelsky, S. Maguire, N. J. Henson, I. Korobkov, B. L. Scott, J. C. Gordon, R. T. Baker and M. Murugesu, *J. Am. Chem. Soc.*, 2011, **133**, 15806–15809.
- 12 A. Eichhöfer, Y. Lan, V. Mereacre, T. Bodenstein and F. Weigend, *Inorg. Chem.*, 2014, **53**, 1962–1974.
- 13 W. H. Harman, T. D. Harris, D. E. Freedman, H. Fong, A. Chang, J. D. Rinehart, A. Ozarowski, M. T. Sougrati, F. Grandjean, G. J. Long, J. R. Long and C. J. Chang, *J. Am. Chem. Soc.*, 2010, **132**, 18115–18126.
- 14 D. E. Freedman, W. H. Harman, T. D. Harris, G. J. Long, C. J. Chang and J. R. Long, *J. Am. Chem. Soc.*, 2010, **132**, 1224–1225.
- 15 C. Mathonière, H.-J. Lin, D. Siretanu, R. Clérac and J. M. Smith, *J. Am. Chem. Soc.*, 2013, **135**,

19083–19086.

- 16 C. G. Werncke, M.-A. Bouammali, J. Baumard, N. Suaud, C. Martins, N. Guihéry, L. Vendier, J. Zheng, J.-B. Sortais, C. Darcel, S. Sabo-Etienne, J.-P. Sutter, S. Bontemps and C. Pichon, *Inorg. Chem.*, 2016, **55**, 10968–10977.
- 17 K. A. Schulte, K. R. Vignesh and K. R. Dunbar, *Chem. Sci.*, 2018, **9**, 9018–9026.
- 18 D. Pinkowicz, F. J. Birk, M. Magott, K. Schulte and K. R. Dunbar, *Chem. – A Eur. J.*, 2017, **23**, 3548–3552.
- 19 X. Feng, C. Mathonière, I.-R. Jeon, M. Rouzières, A. Ozarowski, M. L. Aubrey, M. I. Gonzalez, R. Clérac and J. R. Long, *J. Am. Chem. Soc.*, 2013, **135**, 15880–15884.
- 20 A. Urtizberea and O. Roubeau, *Chem. Sci.*, 2017, **8**, 2290–2295.
- 21 A. K. Bar, C. Pichon, N. Gogoi, C. Duhayon, S. Ramasesha and J.-P. Sutter, *Chem. Commun.*, 2015, **51**, 3616–3619.
- 22 A. K. Bar, N. Gogoi, C. Pichon, V. M. L. D. P. Goli, M. Thlijeni, C. Duhayon, N. Suaud, N. Guihéry, A.-L. Barra, S. Ramasesha and J.-P. Sutter, *Chem. - A Eur. J.*, 2017, **23**, 4380–4396.
- 23 P. Antal, B. Drahoš, R. Herchel and Z. Trávníček, *Eur. J. Inorg. Chem.*, 2018, 4286–4297.
- 24 G.-L. Li, S.-Q. Wu, L.-F. Zhang, Z. Wang, Z.-W. Ouyang, Z.-H. Ni, S.-Q. Su, Z.-S. Yao, J.-Q. Li and O. Sato, *Inorg. Chem.*, 2017, **56**, 8018–8025.
- 25 J. Xiang, J.-J. Liu, X.-X. Chen, L.-H. Jia, F. Yu, B.-W. Wang, S. Gao and T.-C. Lau, *Chem. Commun.*, 2017, **53**, 1474–1477.
- 26 X.-X. Jin, X.-X. Chen, J. Xiang, Y.-Z. Chen, L.-H. Jia, B.-W. Wang, S.-C. Cheng, X. Zhou, C.-F. Leung and S. Gao, *Inorg. Chem.*, 2018, **57**, 3761–3774.
- 27 F. Neese, *Wiley Interdiscip. Rev. Comput. Mol. Sci.*, 2018, **8**, e1327.
- 28 C. van Wüllen, *J. Chem. Phys.*, 1998, **109**, 392–399.
- 29 R. Maurice, R. Bastardis, C. de Graaf, N. Suaud, T. Mallah and N. Guihéry, *J. Chem. Theory Comput.*, 2009, **5**, 2977–2984.